Polymer 210 (2020) 123075

Contents lists available at ScienceDirect

Polymer

journal homepage: http://www.elsevier.com/locate/polymer

Size-dependent phase separation and thermomechanical properties of thermoplastic polyurethanes

Chien-Hsin Wu [a,b], Ying-Chi Huang [a,b], Wei-Lun Chen [a,b], Yen-Yu Lin [a,b], Shenghong A. Dai [c], Shih-Huang Tung [a,b,*], Ru-Jong Jeng [a,b,**]

[a] Institute of Polymer Science and Engineering, National Taiwan University, Taipei, 106319, Taiwan
[b] Advanced Research Center for Green Materials, National Taiwan University, Taipei 106319, Taiwan
[c] Department of Chemical Engineering, National Chung Hsing University, Taichung 402204, Taiwan

ARTICLE INFO

Keywords:
Structure-property
Polyurethanes
Dendrons
Adamantane
Shape memory polymer

ABSTRACT

Over the years, the manipulation of polymer microphase separation associated with molecular architectures has been holding great promise for rendering structure-property relationship. A series of poly (urea/malonamide) dendrons bearing rigid adamantanes in the periphery were developed to serve as branching hard segments (HS) for thermoplastic polyurethanes (TPUs) either in end-capping or pendant manner. Thermal properties, crystalline structures, and mechanical properties of the TPUs were investigated by DSC, X-ray scattering, and DMA, respectively. The introduction of the branching units with bulky adamantanes would expectedly hinder the crystallization of HS. Intriguingly, the dendrons not only accelerate the crystallization of the soft segment (SS, based on polycaprolactone polyol (PCL)), but promote the phase separation between HS and SS to form distinct microdomains as well. These enhanced effects revealed a size-dependent relationship with growing size (or generation) of the branching HS. With the high SS crystallinity that can freeze the chain mobility and the robust HS domains that work as the physical crosslinking points, the resulting TPUs incorporated with adamantane-bearing units show superior shape memory behaviors. This work demonstrates that the molecular engineering on the architectures can significantly tailor the microstructures and properties of thermal plastic polymers.

1. Introduction

The manipulation of microphase separation for polymers with two or more components presents itself a great opportunity to bring about unique properties that are not ever present for a single macromolecule. In thin-films, nanoscale phase separation is often desirable for better device performance. The optimum efficiency in organic photovoltaics depends not only on the use of semi-conductive materials, but on the sophisticated morphologies through interfacial engineering for the charge generation and transportation as well [1,2]. In another field, the utilization of polymeric phase separation for making the bicontinuous porous structures has been realized in the presence of block copolymers that serve as templates for functional materials. In addition to sophisticated synthetic techniques, the etching process generated interconnected meso- or micropores, readily leading to tunable membranes or high capacitances electrode for advanced electrochemical energy storage [3–5].

The unique phase separation and crystallization are of great significance to thermoplastic polyurethanes (TPUs). Unlike traditional thermoset rubber with cross-linked networks, TPUs are capable of exhibiting elastomeric properties that are fully thermoplastic. These unique physical properties and excellent processibility are mainly attributed from two physical chemistry processes of TPUs, one is the strong hydrogen-bonding between urethane linkages; the other is the existence of phase separation between the hard segments (HS) and soft segments (SS). Over the years there have been continuing interests on the manipulation of TPUs properties through the design of polymer architecture [6–8], block length and chemical nature of feedstocks [9,10] and compositions especially regarding HS/SS ratios [11,12] to achieve the desired flexibility, surface characteristics and bulk properties. In one example, TPUs based on rigid aromatic diisocyanates generally result in a higher tensile strength and modulus over the ones based on aliphatic diisocyanates due to the direct association of isocyanate group with phenyl ring [13]. Precisely controlled structures such as the HS of uniform length were

* Corresponding author. Institute of Polymer Science and Engineering, National Taiwan University, Taipei 106319, Taiwan.
** Corresponding author. Institute of Polymer Science and Engineering, National Taiwan University, Taipei 106319, Taiwan.
E-mail addresses: shtung@ntu.edu.tw (S.-H. Tung), rujong@ntu.edu.tw (R.-J. Jeng).

https://doi.org/10.1016/j.polymer.2020.123075
Received 24 June 2020; Received in revised form 16 September 2020; Accepted 20 September 2020
Available online 24 September 2020
0032-3861/

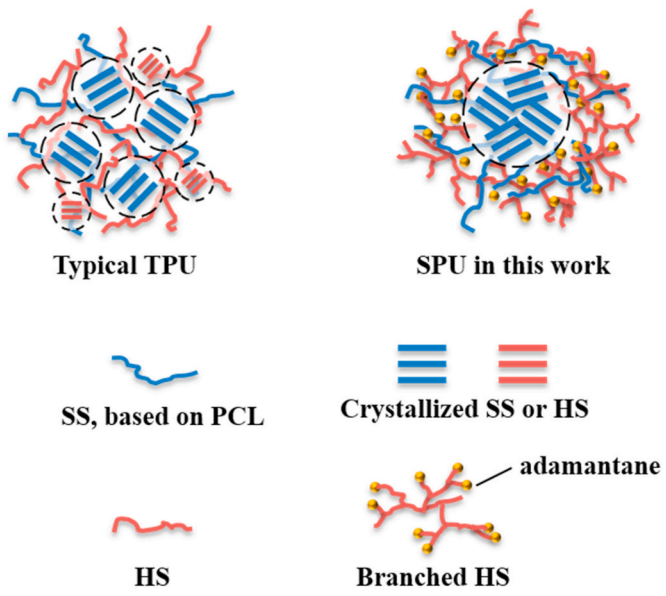

Scheme 1. Illustration of typical and size-dependent thermoplastic polyurethanes.

utilized to facilitate the microphase separation, leading to higher modulus and elongation at break for TPUs [14–18]. However, the above-mentioned morphological engineering through balancing the ratios of HS to SS often gets bogged down by disproportional crystallinity and phase separation. Previously, our lab attempted to develop a methodology to enhance the TPU properties via the introduction of HS pendants with different iterative units [19]. It was found that the use of the pendants with either linear or dendritic structures would lead to the slow formation of SS crystallinity in TPUs. Moreover, these amorphous HS quickly disintegrated for lack of physical crosslinking junctions when the temperature was higher than the T_m of SS, due to the presence of the disrupted polymer chain packing by the branching HS in TPUs. Indeed, the control of phase separation as well as the morphology fixation are extremely difficult to achieve. Based on the above, a thorough study on structure-property relationships of TPUs in terms of the impacts of different hard segments with precise chain lengths on the thermal and mechanical properties remains to be a challenging task.

It was reported that the introduction of adamantyl moieties (acting as organic fillers) to polymers would bring about unique structure-properties relationship in the areas of the thermal behavior, phase separation morphology and mechanical properties [20–22]. In most cases, the adamantane containing TPUs exhibited amorphous microstructures. This is because its cubic geometry nanostructure would prevent the polymer chains from regular organization into crystalline domain [23–25]. Nevertheless, by utilizing multiple functional adamantyl moieties along with an optimized chemically cross-linking density for PUs, robust thermal and mechanical properties as well as specific performances such as shape memory effect were realized. In addition, Chen et al. [26] suggested a strategy by using star-branched segments composed of adamantane as the core, and poly (ε-caprolactone) segments (PCL segment) as the arm to achieve polyurethane frameworks with semi-crystalline properties. Interestingly, the improved crystallization ability of the adamantane containing PCL segments was observed when compared with the pristine PCL segments as evidenced by a higher crystal melting peak and a larger melting enthalpy. This is because the rigid adamantane would be able to serve as nucleus for crystallization of PCL segments [26]. Although the enhancement of the mechanical properties of resulting PUs was limited by the presence of the extremely low adamantane content, shape memory properties of 99% shape fixation and 85% shape recovery were achieved.

In our previous effort, a dual-functional building intermediate, 4-(3,3-diethyl-2,4-dioxoazetidin-1-yl)benzoyl chloride, or 4-isocyanate-4′-(3,3-dimethyl-2,4-dioxo-azetidine)diphenyl methane (IDD) was developed for the preparation of well-defined chain extenders for TPUs [27–32]. With a highly reactive isocyanate unit on one end, and a selectively reactive azetidine-2,4-dione on the other end, the IDD based hard segments with well-defined chain length and multiple hydrogen bonding sites were realized, demonstrating that supramolecular structures could be created via macromolecular architecture [33–36]. These reactions featured high yield under mild conditions in the absence of harsh reagents such as phosgene, or painstaking protection/deprotection procedures. In this study, a strategy of manipulating the polymer phase separation for sustaining robust HS domains in the semi-crystalline TPUs is revealed in Scheme 1. Via tailoring the branching sizes, the cage-like adamantyl moieties were introduced in the periphery of dendritic architectures to create thermodynamic incompatibility between HS and SS segments [26]. The subsequent incorporation of dendritic structures as chain extenders provided a series of TPUs with different well-defined branching side groups for the investigation of structure-properties relationship. Comparing to typical TPUs with micro-phase separation of crystallized SS and crystalized HS, TPUs prepared in this study have branching size-dependent crystallinity domain of SS. Thanks to the bulky size of adamantyl moieties capable of acting as nucleating site for crystallization of PCL based SS while creating distinguished microphase separation, these TPUs exhibited sharp melting transitions and lengthy rubbery plateaus fit for the applications of shape memory materials [37–39].

2. Results and discussion

2.1. Synthesis and characterization of dendrons and dendritic chain extenders

The preparation of adamantane containing dendritic hard segments were carried out based on the dual-functional 4-isocyanate-4′-(3,3-dimethyl-2,4-dioxo-azetidine)diphenyl methane (IDD) compound, bearing the highly reactive isocyanate group active toward hydrogen such as hydroxyl- or amino-group, and the selectively reactive azetidine-2,4-dione unit active toward only aliphatic primary amine (such as diethylenetramine, DETA) (Scheme 2). The adamantane containing poly (urea/malonamide) dendrons of generation 0.5 to 2.5 are denoted as [G0.5]-ada, [G1.0]-ada, [G1.5]-ada, [G2.0]-ada, and [G2.5]-ada. Subsequently, [G0.5]-ada, [G1.5]-ada, and [G2.5]-ada were respectively modified with 6-amino-1-hexanol to obtain a series of end-capping agents with primary alcohol functional groups, which are denoted as E−[G0.5]-ada, E−[G1.5]-ada, and E−[G2.5]-ada). Likewise, the dendrons were respectively modified with N-(3-amino-propyl)diethanolamine (APDEA) to form the dendritic chain extenders with diol functional groups, which are denoted as A-[G0.5]-ada, A-[G1.5]-ada, and A-[G2.5]-ada.

For the preparation of dendrons, the first step is peripheral functionalization of IDD (Scheme 2). This reaction involves reacting isocyanates to various nucleophiles with facileness due to the positive charge on the carbon atom polarized by the high electronegativity of nitrogen and oxygen atoms of –N═C═O group. In spite of that, various nucleophilic reagents would exhibit different reactivities toward isocyanates depending on the nature of nucleophilic centers. In one example, the isocyanate group is reactive toward primary alcohols or primary amino functional groups. Yet, the isocyanate is 1000 times more reactive toward the primary amine groups than the primary alcohols [40]. This is further corroborated by our previous studies [27–32]. Nevertheless, an extremely low reactivity between isocyanate functional group and the primary alcohol on the adamantyl moieties was observed in the peripheral functionalization. The isocyanate exhibited virtually no reactivity toward 1-adamantanol after heating at 60 °C for 3 h as shown in the model reaction by using ^{1}H NMR titration (Figure S1). In fact, the adamantyl characteristic chemical shifts of 1-adamantanol

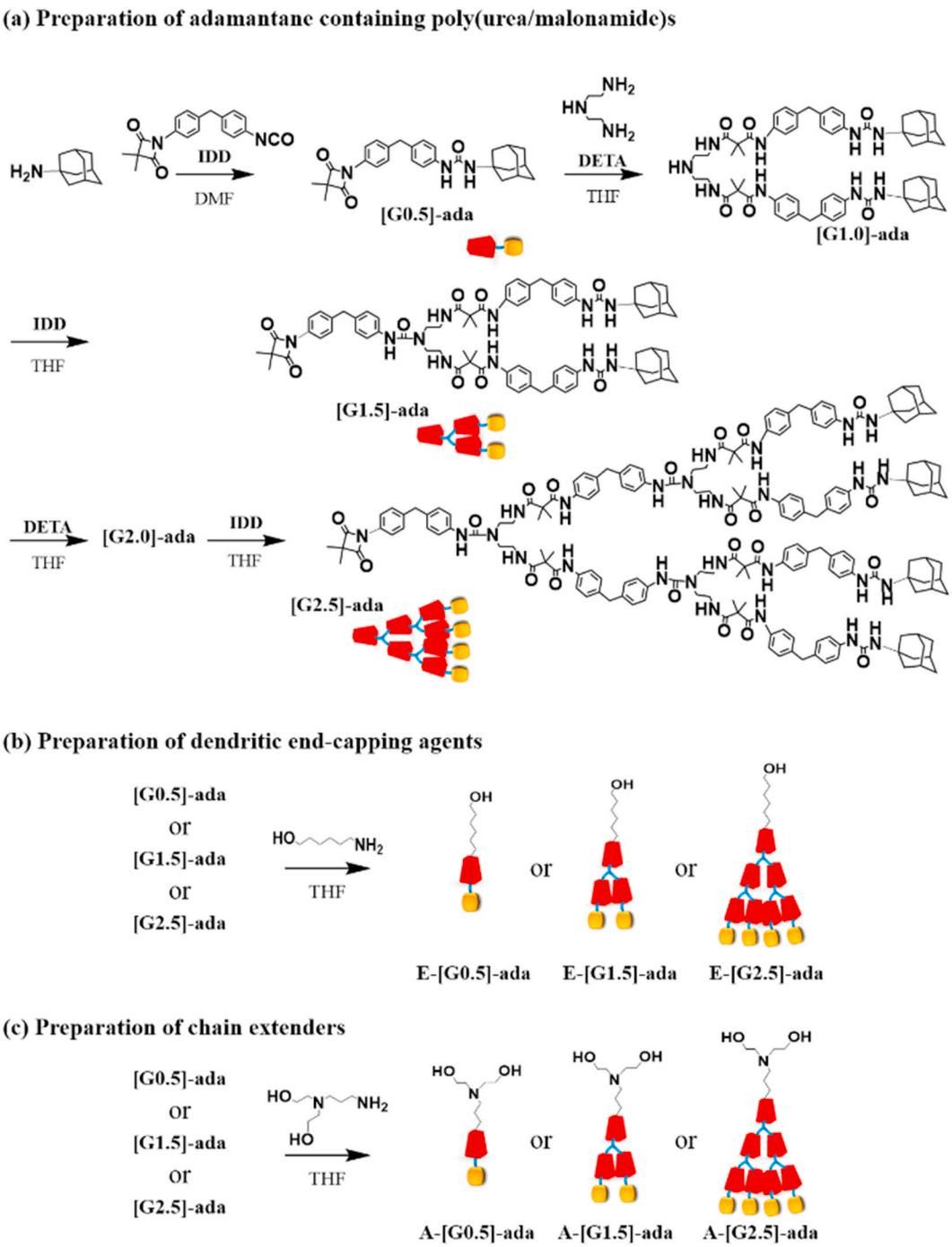

Scheme 2. Preparation of (a) adamantane containing poly (urea/malonamide)s, (b) end-capping agents, and (c) chain extenders.

(1.65 and 2.08 ppm) remained intact after reacting with phenyl isocyanate. This is due to the fact that the existence of steric hindrance effect plays a major role in reducing the reactivity of isocyanate toward the active hydrogen closely attached to the bulky adamantyl moiety [41]. Based on this consideration, compound 1-adamantanamine with much better reactivity toward isocyanate was chosen to be the reagent for the peripheral functionalization. The reaction between 1-adamantanamine and phenyl isocyanate was monitored by ^{1}H NMR titration (Figure S2). The adamantyl characteristic chemical shifts of 1-adamantanamine (1.56, 1.60–1.75, and 2.02 ppm) were shifted to 1.75 and 2.05 ppm, indicating the completion of the functionalization.

Indeed, the peripheral functionalization required a highly reactive nucleophile, i.e. 1-adamantanamine, to overcome the steric hindrance effect from the adamantyl moiety. However, the compounds with aliphatic primary amine groups are reactive toward both the isocyanate and azetidine-2,4-dione functional group on the dual-functional IDD compound [27,29]. This implies that the possible end-capping reactions of IDD with adamantyl moieties would occur through isocyanate and azetidine-2,4-dione during peripheral functionalization. Nevertheless, the steric hindrance effect turned out to be a boon to circumvent this issue. Due to the presence of the steric hindrance effect, the aliphatic primary amine of 1-adamantanamine was not reactive toward azetidine-2,4-dione. Instead, the aliphatic primary amine only reacted to the isocyanate group. For the synthesis of [G-0.5]-ada, the reaction was monitored by ^{1}H NMR. The adamantyl characteristic peaks were shifted to 1.57, 1.86, and 1.96 ppm after the reaction. The newly formed peaks

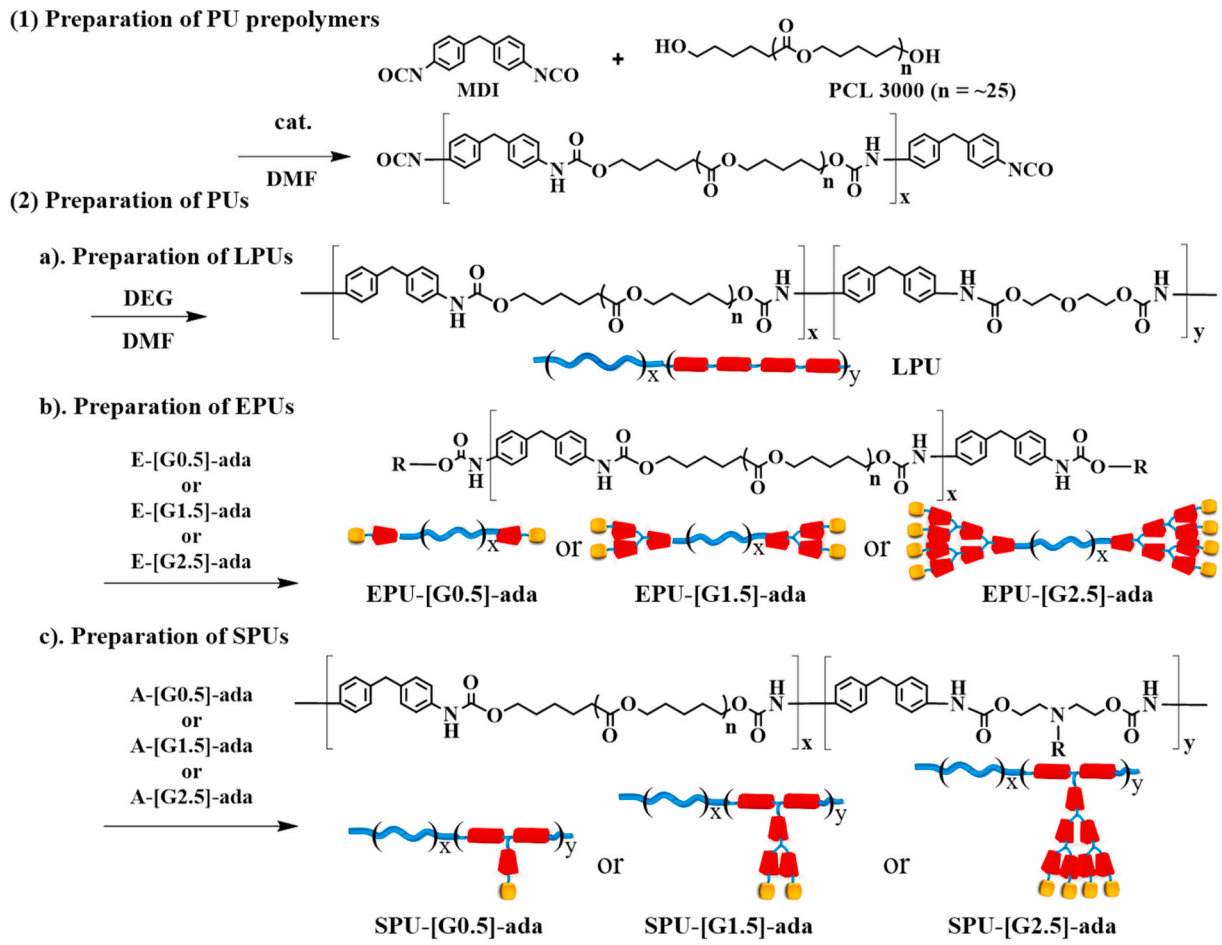

Scheme 3. Polymerization of linear, end-capped, and dendritic PUs.

were appeared at 5.75 and 8.15 ppm of the urea group for the purified [G-0.5]-ada product (Figure S3). A high yield of 90% was achieved. Subsequently, [G-0.5]-ada was reacted with diethyltriamine (DETA) for the preparation of [G-1.0]-ada. It is important to note that the virtually linear generation 1.0 poly (urea/malonamide)s with dense polar sites usually leads to poor solubility unfit for the ^{1}H NMR measurement [27, 29–31]. Fortunately, by the following addition of the IDD to prepare a branched generation 1.5 poly (urea/malonamide)s, the [G-1.5]-ada product exhibited good solubility in solvents such as THF and DMSO for the ^{1}H NMR measurement. As shown in Figure S4, two methylene peaks were split at 3.72 and 3.79 ppm with an integral ratio of 4 to 2. The [G-1.5]-ada sample was further reacted with DETA and IDD in sequence to obtained [G-2.0]-ada and [G-2.5]-ada, respectively. For [G-2.0]-ada, only one methylene peak was observed at 3.71 ppm (Figure S5), whereas two methylene peaks were split at 3.72 and 3.79 ppm with an integral ratio of 12 to 2 for [G-2.5]-ada (Figure S6). ^{1}H NMR, EA, Mass and GPC results are shown in Table S1.

2.2. Synthesis and characterization of dendritic polyurethanes

In order to incorporate the adamantane containing poly (urea/malonamide)s into the polyurethanes, the dendrons were modified with either primary alcohol moieties as end-capping agents (denoted as E−[G0.5]-ada, E−[G1.5]-ada, and E−[G2.5]-ada for generation 0.5, 1.5, and 2.5, respectively), or diol moieties as chain extenders (denoted as A-[G0.5]-ada, A-[G1.5]-ada, and A-[G2.5]-ada for generation 0.5, 1.5, and 2.5, respectively; Scheme 2). For the end-capping agents, the reactions were carried out by the addition of 6-amino-1-hexanol, the reagent with a primary amine and a primary alcohol, to [G0.5]-ada, [G1.5]-ada, or [G2.5]-ada. As shown in ^{1}H NMR spectra (Figure S7-S9), E−[G0.5]-ada, E−[G1.5]-ada, and E−[G2.5]-ada were achieved as evidenced by the disappearance of two splitting peaks at 3.72 and 3.79 ppm, and the newly shifted methylene peak at 3.72 ppm. Similarly, for dendritic chain extenders, the reactions were carried out by the respective addition of APDEA to [G0.5]-ada, [G1.5]-ada, and [G2.5]-ada. Through the reaction between the azetidine-2,4-dione and the primary amine, the dendritic chain extenders with diol functional groups (A-[G0.5]-ada, A-[G1.5]-ada, and A-[G2.5]-ada) were obtained as indicated by the disappearance of two splitting peaks at 3.71 and 3.78 ppm, and the newly shifted methylene peak at 3.72 ppm (Figure S10-S12). These reactions were also monitored by using FT-IR spectra (Figure S13). During the preparation of dendrons, the absorption peaks at 1742 cm^{-1} and 1856 cm^{-1} indicates the formation of azetidine-2,4-dione functional groups for the compounds of [G0.5]-ada, [G1.5]-ada, and [G2.5]-ada (Figure S13(a)). In addition, the successful ring opening reaction of azetidine-2,4-dione moiety by the primary amine group was evidenced by the disappearance of absorption peaks at 1742 cm^{-1} and 1856 cm^{-1} and the emergence of a malonamide absorption peak at 1656 cm^{-1}. For the preparation of chain extenders and end-capping agents such as E−[G2.5]-ada and A-[G2.5]-ada, the disappeared azetidine-2,4-dione absorption peaks at 1742 cm^{-1} and 1856 cm^{-1} indicates the completed reaction of [G-2.5]-ada to 6-amino-1-hexanol or APDEA, while the newly emerge malonamide and hydroxyl peaks at 1656 cm^{-1} and 3350 $\pm$ 50 cm^{-1}, respectively, indicates the presence of the target compounds (Figure S13(b)). EA, Mass and GPC results are shown in Table S1.

The introduction of bulky side-groups or end-capping agents composed of adamantane containing poly (urea/malonamide)s to TPUs was accomplished by a typical two-step polymerization (Scheme 3). For

Table 1
Formulations, compositions and properties of TPUs.

Sample[a]	MDI[b] (mol)	Polyol[c] (mol)	Chain extenders (mol)			Ada%[g] (wt%)	M_w[h] (g/mol × 10^4)	Đ[h]	$X_{C1,SS}$[i] (%)	$X_{C2,SS}$[i] (%)
			DEG[d]	Dendritic diols[e]	End-capping agents[f]					
LPU35	1.26	0.26	1	0	0	0.0	8.5	4.10	60.3	23.7
LPU40	1.20	0.20	1	0	0	0.0	9.8	3.43	45.4	0.0
LPU45	1.16	0.16	1	0	0	0.0	7.5	3.18	36.5	0.0
LPU50	1.13	0.13	1	0	0	0.0	10.7	3.29	0.0	0.0
LPU55	1.10	0.10	1	0	0	0.0	12.1	3.60	0.0	0.0
EPU45-[G0.5]	1.65	0.65	0	0	2	3.8	2.1	1.71	12.1	0.0
EPU55-[G0.5]	1.42	0.26	0	0	2	6.0	1.3	1.58	74.5	0.0
EPU45-[G1.5]	2.46	1.46	0	0	2	3.4	1.8	2.02	79.7	69.8
EPU55-[G1.5]	1.94	0.94	0	0	2	4.3	1.2	1.73	82.6	5.6
EPU45-[G2.5]	4.08	3.08	0	0	2	3.2	1.9	1.89	38.5	71.5
EPU55-[G2.5]	2.99	1.99	0	0	2	4.1	1.6	1.50	51.4	71.3
SPU45-[G0.5]	1.40	0.40	0	1	0	6.2	8.2	3.55	86.5	0.0
SPU50-[G0.5]	1.32	0.32	0	1	0	7.1	7.3	2.90	83.1	0.0
SPU55-[G0.5]	1.26	0.26	0	1	0	7.9	6.8	3.67	81.2	0.0
SPU35-[G1.5]	2.30	1.30	0	1	0	4.5	7.4	2.89	94.1	52.7
SPU40-[G1.5]	2.02	1.02	0	1	0	5.3	9.1	3.70	91.6	40.2
SPU45-[G1.5]	1.81	0.81	0	1	0	6.2	8.9	2.81	78.8	29.5
SPU50-[G1.5]	1.66	0.66	0	1	0	6.9	7.3	2.94	36.6	8.2
SPU55-[G1.5]	1.52	0.52	0	1	0	7.8	8.6	3.50	23.7	0.0
SPU35-[G2.5]	3.61	2.62	0	1	0	4.5	8.2	2.77	66.3	51.4
SPU40-[G2.5]	3.04	2.04	0	1	0	5.3	9.0	3.20	77.7	50.8
SPU45-[G2.5]	2.62	1.62	0	1	0	6.2	8.7	3.09	54.6	50.4
SPU50-[G2.5]	2.30	1.30	0	1	0	7.0	8.1	3.41	32.2	53.5
SPU55-[G2.5]	2.04	1.04	0	1	0	7.8	7.0	2.65	0.0	33.4

[a] The hard segment contents (HS%) are calculated according to the following formula: HS%= (MDI (g)+chain extenders(g))/(overall PU(g)).
[b] The molecular weight of MDI is 250.25 (g/mol).
[c] The molecular weight of polycaprolactone polyol (PCL3000) is 3000 (g/mol).
[d] The molecular weight of diethylene glycol (DEG) is 106.12 (g/mol).
[e] The molecular weights of dendritic chain extenders are 633.4 (g/mol), 1527.9 (g/mol), and 3316.8 (g/mol) for A-[G0.5]-ada, A-[G1.5]-ada, and A-[G2.5]-ada, respectively.
[f] The molecular weights of dendritic end-cappers are 588.4 (g/mol), 1482.9 (g/mol), and 3271.8 (g/mol) for E−[G0.5]-ada, E−[G1.5]-ada, and E−[G2.5]-ada, respectively.
[g] The weight ratios (wt%) of adamantly moieties in PUs.
[h] Weight average molecular weight (M_w) and polydispersity (Đ) were measured by using the GPC.
[i] The crystallinity of PCL based soft segments for TPUs ($X_{C1,SS}$ and $X_{C2,SS}$) were investigated by measuring melting enthalpy during the first and second heating run in DSC, respectively; and calculated according to the formula ($\triangle H_{m,\ SS}/\triangle H_{m,\ PCL}$,100 %) × 100 %, where $\triangle H_{m,\ PCL}$ is the melting enthalpy of PCL (82.9 J/g).

the PU prepolymer preparation, the polyester based polyol of polycaprolactone with a molecular weight of 3000 g/mol was reacted with MDI at 60 °C for 0.5 h in the presence of tin catalyst. Subsequently, the PU prepolymers were further reacted with dendritic end-capping agents (E−[G0.5]-ada, E−[G1.5]-ada, and E−[G2.5]-ada) or chain extenders (A-[G0.5]-ada, A-[G1.5]-ada, and A-[G2.5]-ada). As a result, a series of dendritic TPUs were obtained, including the ones with dendritic end-capping dendritic structures (EPU), and side-chained structures (SPU), The EPUs end-capped by E−[G0.5]-ada, E−[G1.5]-ada, or E−[G2.5]-ada would be denoted as EPU-[G0.5]s, EPU-[G1.5]s, or EPU-[G2.5], respectively. On the other hand, SPUs chain-extended by A-[G0.5]-ada, A-[G1.5]-ada, or A-[G2.5]-ada would be denoted as SPU-[G0.5], SPU-[G1.5], or SPU-[G2.5], respectively. For the sake of reference, a TPU with a linear structure (LPU) was also prepared. The compositions between HS/SS were studied and designated as LPUxx for LPUs, SPUxx-[G0.5] for SPU-[G0.5]s, SPUxx-[G1.5] for SPU-[G1.5]s, SPUxx-[G2.5] for SPU-[G2.5]s, and EPUxx-[G0.5] for EPU-[G0.5]s, EPUxx-[G1.5] for EPU-[G1.5]s, and EPUxx-[G2.5] for EPU-[G2.5]s, and SPUxx-[G0.5] for SPU-[G0.5]s, SPUxx-[G1.5] for SPU-[G1.5]s, SPUxx-[G2.5] for SPU-[G2.5]s; where the numbers are the weight ratio of hard segment (HS %) contents calculated by HS%= (MDI (g)+chain extenders(g))/(overall PU(g)).

In general, GPC measurement provides relative molecular weight and the polydispersity (Đ) calibrated by using monodisperse linear polymers such as polystyrene as standard. However, comparing to typical linear polymers with random-coil conformation in polymer solution, the repetitively branched tree-like molecules exhibited higher density in the increased molecular weight from GPC measurements [42,43]. Due to the fact that the GPC analysis is based on various hydrodynamic volumes, depending on the type of functional group or the selection of solvents. Consequently, GPC appears to be less sensitive in terms of detecting structural differences for highly branched polymer structure such as dendrimer in the literature [44,45]. As a result, the conventional molecular weight determination method by using calibration curve cannot be used in such cases.

Nevertheless, GPC measurement is a facile method to evaluate the molecular weight distribution (Đ) in the development of dendritic structures [46,47]. As shown on page 10, Table S1 of Supporting Information, the low values of molecular weight distribution (Đ <1.05) indicate the purity and monodispersity for dendrons and dendritic chain extenders. Mass spectroscopy such as ESI (electrospray ionization) or MALDI (matrix-assisted laser desorption ionization) in combination with a time of flight mass spectrometer (TOF MS) were also utilized to determine the empirical molecular weights, along with the results of elemental analysis (EA) providing the evidence to the weight percent of each element from calculated number. The structures of target compounds could thus be established [42–47].

The synthesis of TPUs was characterized by using FT-IR. For LPU50, the presence of the absorption peaks at 1727 cm^{-1} and 1702 cm^{-1} for free carbonyl group and hydrogen-bonded carbonyl group, respectively, confirmed the formation of urethane linkages (Figure S13(b)) [48,49]. Furthermore, the dendron containing EPU50-[G2.5] and SPU50-[G2.5] exhibited urethane carbonyl absorption peaks at 1723 cm^{-1} and 1726 cm^{-1}, respectively. The absorption peaks at about 1650 cm^{-1} were attributed to the presence of malonamide linkages of the dendritic E−[G2.5]-ada and A-[G2.5]-ada. The molecular weights were measured by

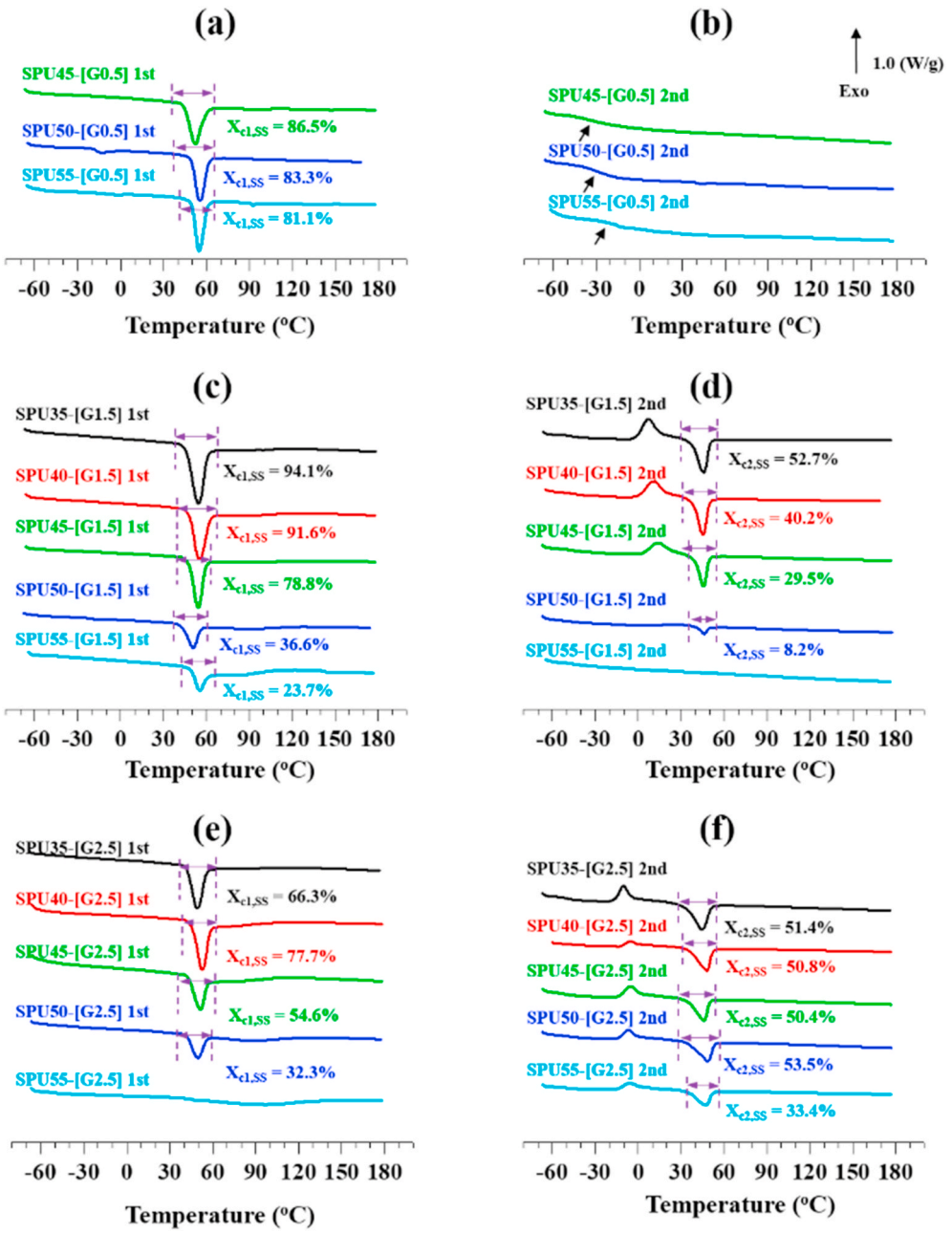

Fig. 1. DSC thermograms from the first heating run for (a) LPUs, (c) SPU-[G1.5]s, and (e) SPU-[G2.5]s; and the second heating run for (b) LPUs, (d) SPU-[G1.5]s, and (f) SPU-[G2.5]s.

gel permeation chromatography (GPC) in DMF as eluent and calibrated by using polystyrene as standards (Table 1). The weight average molecular weights (M_ws) ranged from 75,000 to 120,000 g/mol, with polydispersities (Đ) between 3.2 and 4.1 for LPUs; M_ws ranged from 13,000 to 21,000 g/mol with Đ in the range of 1.5–2.1 for EPUs; M_ws ranged from 68,000 to 91,000 g/mol with polydispersities in the range of 2.6–3.7 for SPUs. Relatively low molecular weights for EPUs are because EPUs were derived from the end-capping reactions of the PU prepolymers, i.e. the PU prepolymers were not chain-extended in this case. The formulations, compositions and molecular weight are listed in Table 1.

2.3. Thermal properties and phase separation

Thermal properties of adamantane containing poly (urea/malonamide)s were studied using thermogravimetric analysis (TGA) and differential scanning calorimetry (DSC) as shown in Figure S14. For the TGA analysis, the samples were equilibrated at 105 °C for 30 min in the furnace to remove moisture first, and temperature was ramped from 105 to 800 °C at a heating rate of 10 °C/min under nitrogen. All the dendrons exhibited a 5% weight loss temperature higher than 185 °C. For the DSC analysis, the thermal phase transitions were investigated with the second heating scans at a rate of 10 °C/min under nitrogen (Figure S14). No apparent transition was found for [G0.5]-ada below 200 °C. This is different from the dendrons of generations 0.5 bearing peripheral linear alkyl chains or phenyl groups that exhibited melting points (T_ms) in our previous studies [19,33]. Moreover, we had found that the dendritic poly (urea/malonamide)s with higher generations only showed distinct glass transition T_g which increased as the dendron increased in size [28]. In this work, due to the presence of the rigid adamantane moieties in the periphery that would restrict the molecular motion, the T_g of [G2.5]-ada reached to 178 °C, much higher than those of the counterparts with peripheral alkyl chains or phenyl groups [19]. All the dendritic poly

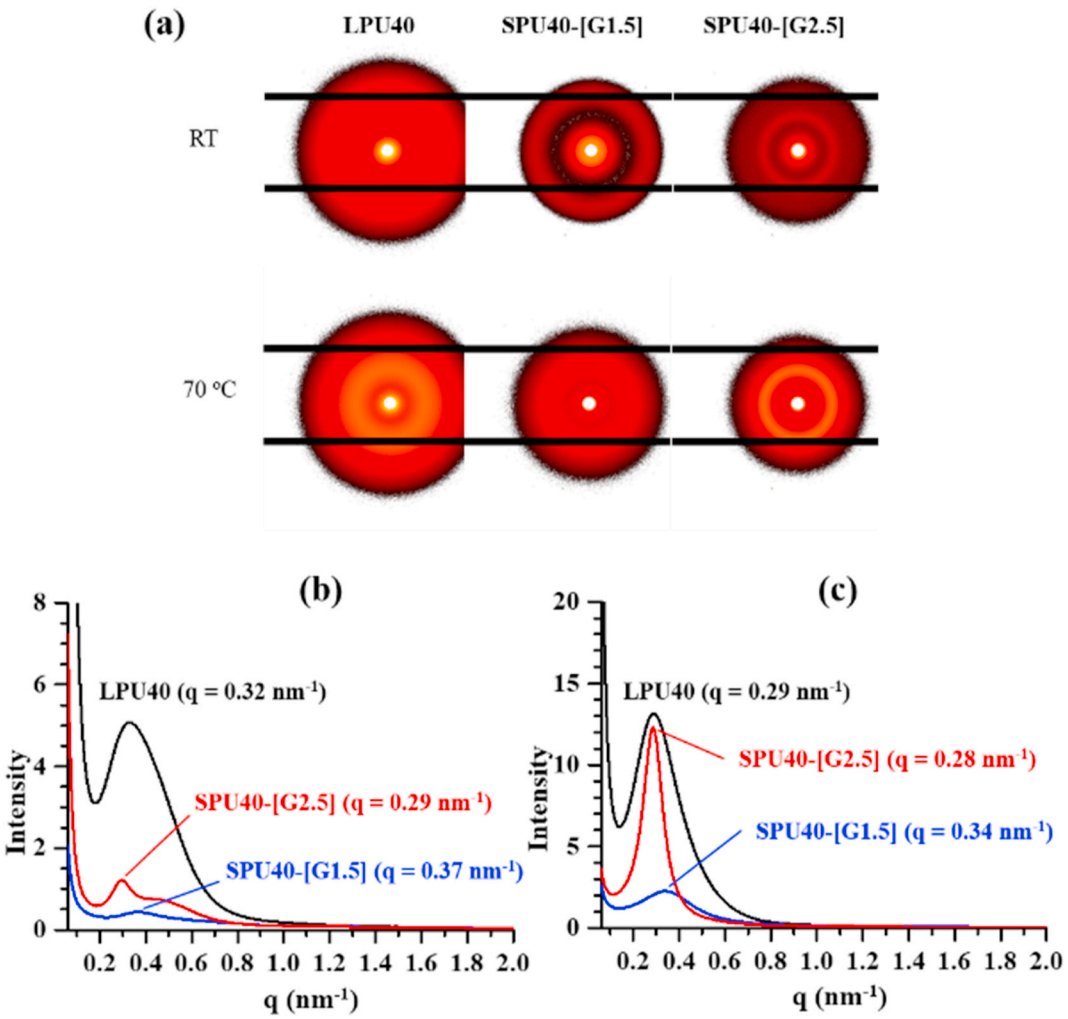

Fig. 2. Small-angle X-ray scattering (SAXS) of (a) 2-D patterns of TPU with 40 wt% HS at RT and 70 °C, and the corresponding 1-D profiles at (b) RT and (c)70 °C, respectively.

(urea/malonamide)s exhibited only amorphous phase without any sign of crystallinity. This is possibly due to the fact that the bulky adamantanes would disrupt the molecular packing.

DSC thermograms of LPUs with linear architecture for the first and the second heating runs at a rate of 10 °C/min are shown in Figure S15. LPU35, LPU44, and LPU45 exhibited typical semi-crystalline TPU properties. The first heating runs in Figure S15(a) showed sharp endothermic melting peaks at ~ 50 °C ($T_{m,SS}$) that are assigned to the crystalline PCL-based SS [50] and the broad transitions at temperatures above 150 °C were the melting of HS ($T_{m,HS}$) [51]. When the ratio of HS content increased, the degree of SS crystallinity calculated from the melting transition of the first heating run ($X_{c1,SS}$) decreased 60.3%, 45.4%, 36.5%, 0.0% and 0.0% for LPU35, LPU40, LPU45, LPU50, and LPU55, respectively. $T_{m,HS}$ increased with increasing HS content from about 150 °C to 185 °C. This result implies that the SS and HS in LPUs crystallized separately and were microphase-separated. For LPU50 and LPU55 with higher HS fractions, the dominant crystallization of HS might fix the LPU chains in an arrangement that favored HS packing but sacrificed the SS packing. This explains why the SS crystallization was absent. In the second heating runs (Figure S15(b)), only LPU35 exhibited a recrystallization and a melting transition of the SS domain ($X_{c2,SS}$ ~ 23.7%). The melting of the HS domain became obscure as well. This indicates that the crystallization of LPUs was suppressed and slow under a 10 °C/min cooling. The glass transition temperature ($T_{g,SS}$) of the SS domain could be therefore clearly observed at ~ −40 °C due to the high fraction of the amorphous phase in these samples.

The introduction of adamantane containing dendrons into the TPUs causes unusual thermal transitions. Different from the previous literature in which the SS crystallization was limited by the introduction of the dendritic poly (urea/malonamide)s with peripheral alkyl chains [19,30,31], the first heating runs of SPUs with side-chain dendritic poly (urea/malonamide)s with peripheral adamantyl moieties exhibited sharper SS melting peaks at ~ 55 °C and higher SS crystallinity in comparison to the LPU counterparts (Fig. 1). In contrast, the melting peak above 150 °C disappeared due to the presence of the bulky side-chain dendrons that retarded the HS crystallization. The SS crystallinity decreased slightly with increasing HS contents and the degrees of crystallinity of SPU-[G0.5] series were over 80% even for the samples with high HS contents such as SPU50-[G0.5] and SPU55-[G0.5] (Fig. 1 (a)). This is due to the fact that the bulky branching units would hinder the HS packing. This in turn gives more freedom to SS for close packing, which becomes dominant so as to lower the free energy [19,30]. For the second heating runs, the crystallization of SPU-[G0.5] series was fully suppressed under a 10 °C/min cooling and $T_{g,SS}$ at ~ −30 °C could be observed due to low crystallinity (Fig. 1(b)).

For the side-chain TPUs with the dendrons of higher generations, SPU-[G1.5] and SPU-[G2.5] series were able to crystallize under cooling (Figure S16) and recrystallize upon heating (Fig. 1), except SPU55-[G1.5]. We suggest two reasons for the higher crystallization rates of SPU-[G1.5] and SPU-[G2.5] series. First, the bulkier side-chain

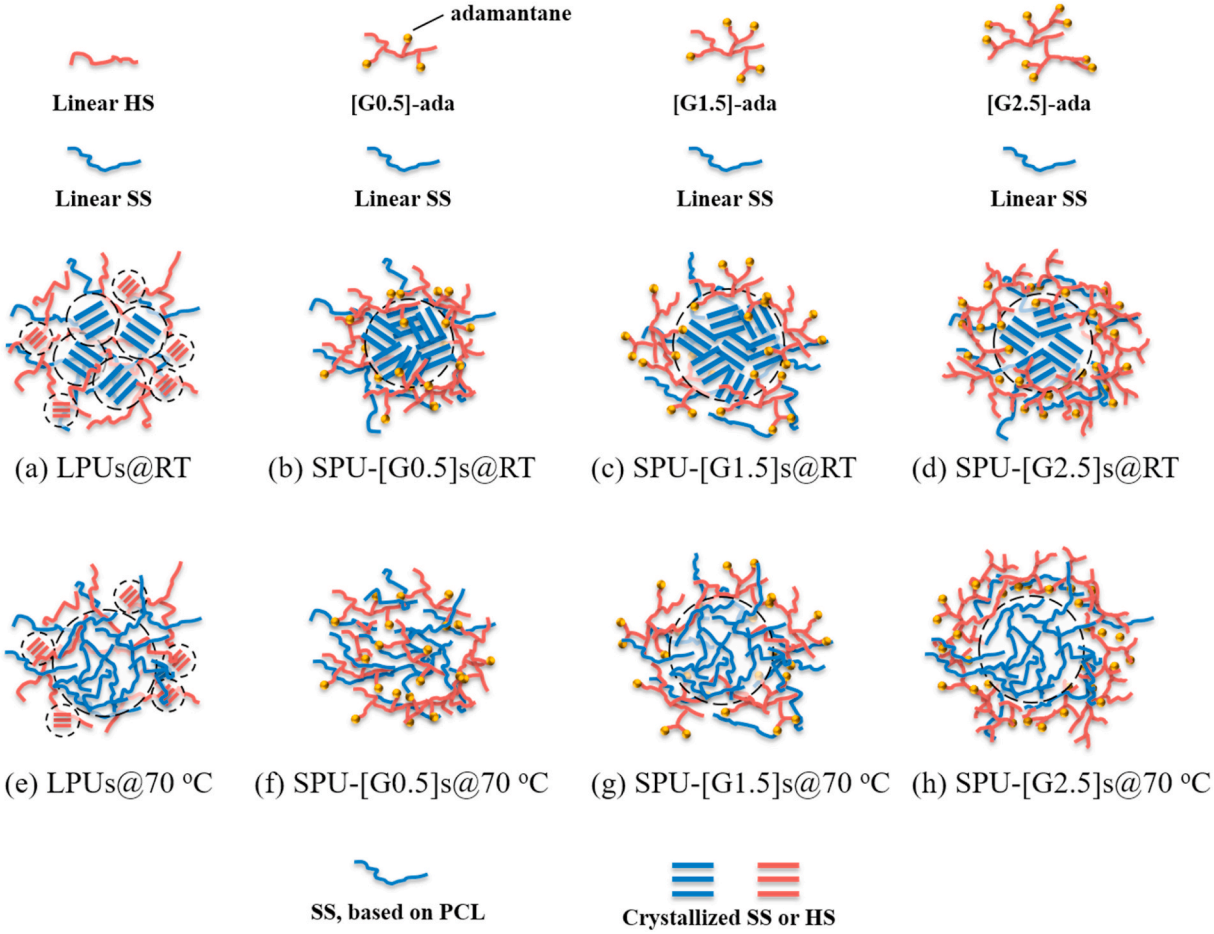

Fig. 3. Size-dependent phase separation morphology of TPU samples at room temperature (a)–(d), and (e)–(h) 70 °C.

dendrons would prevent the HS from close packing, i.e. leading to lower free energy, and therefore the free energy of the system is dominated by the SS crystallization. Second, the dendron of higher generation increases the incompatibility between SS and HS and thus promotes the microphase separation between SS and HS in SPUs at elevated temperatures where the chains can freely move. This would facilitate the SS packing in purer soft domains under cooling as evidenced by the observation of the SPU55-[G2.5] crystallization shown in the second heating after a thermal cycle (Fig. 1(f)) in contrast to the amorphous characteristics observed in the first heating. The EPUs exhibited similar thermal properties to those of SPUs as revealed in Figure S17 even though the dendrons were in the end-capped positions instead of pendant ones. The $T_{g,HS}$ values could be observed at 120 and 140 °C for EPU55-[G1.5] and EPU55-[G2.5], respectively. In summary, the adamantane-containing dendrons on TPUs would certainly suppress the HS packing while favoring the SS packing.

The structures of the TPUs samples were investigated by X-ray diffraction (WXRD) as shown in Figure S18. In Figure S18(a), the diffraction peaks of LPUs at 21.3° and 23.5° were produced by (110) and (200) planes of the PCL-based SS crystals, respectively [52], and the diffraction peaks at 9.6° and 18.8° corresponded to the characteristic peaks of MDI-based HS crystalline domains [51], indicating both SS and HS form crystals. This is in agreement with the DSC results. Comparing to the LPU samples, more distinct peaks with narrower width at 21.3° and 23.5° were found for the branched SPU-[G1.5]s and SPU-[G2.5]s, in the absence of the HS crystal diffraction (Figure S18(b) and (c)). This result suggests that the branched SPUs exhibited only the crystalline SS domains with a higher crystallinity and a more ordered packing over LPUs, also consistent with the DSC results.

The phase-separated morphology of the TPU samples were further investigated by small angle X-ray scattering (SAXS) at room temperature and 70 °C. The 2-D patterns and the corresponding 1-D profiles of the samples with 40 wt% HS are shown in Fig. 2. At room temperature, LPU40 exhibited a circular scattering ring at $q = 0.32$ nm^{-1} (d-spacing = 19.6 nm), a feature of the microphase-separated morphology between SS and HS with random orientation. For the SPUs with dendritic pendants, the d-spacings were 17.0, and 21.7 nm for SPU40-[G1.5] and SPU40-[G2.5], respectively. The d-spacings increased when the SPUs comprised the dendrons of higher generation. At 70 °C, which was over the SS melting temperature, the polymer chains could move freely to reorganize. The diffraction peak of LPU40 became sharper and slightly shifted to a lower q. In the cases of SPU40-[G1.5] and SPU40-[G2.5], the diffraction peaks at 70 °C became much sharper and moved to lower q territory as well, especially for SPU40-[G2.5]. The results imply that more distinct microphase-separated domains composed of pure HS and SS were formed. This is caused by the increasing incompatibility between HS and SS as the SPUs comprised dendrons of higher generation. The purer soft domains allowed SS to pack easily so that the crystallization rate was increased, as evidenced by the DSC results in Fig. 1. It is important to note that the size-dependent behavior of TPU microphase separation was also observed in the nearly disappeared diffraction peak at 70 °C for SPU45-[G0.5], indicating a well mixing of HS and SS after the melting (Figure S19).

At room temperature, TPUs exhibited typical microphase separation for LPUs with 60 wt% or 55 wt% of SS based on the morphology study from DSC and X-ray diffractions. The crystallized SS would phase-separate from the domains comprising the mixing phase of amorphous SS and semi-crystallized HS as shown in Fig. 3(a). At 70 °C, the melted SS

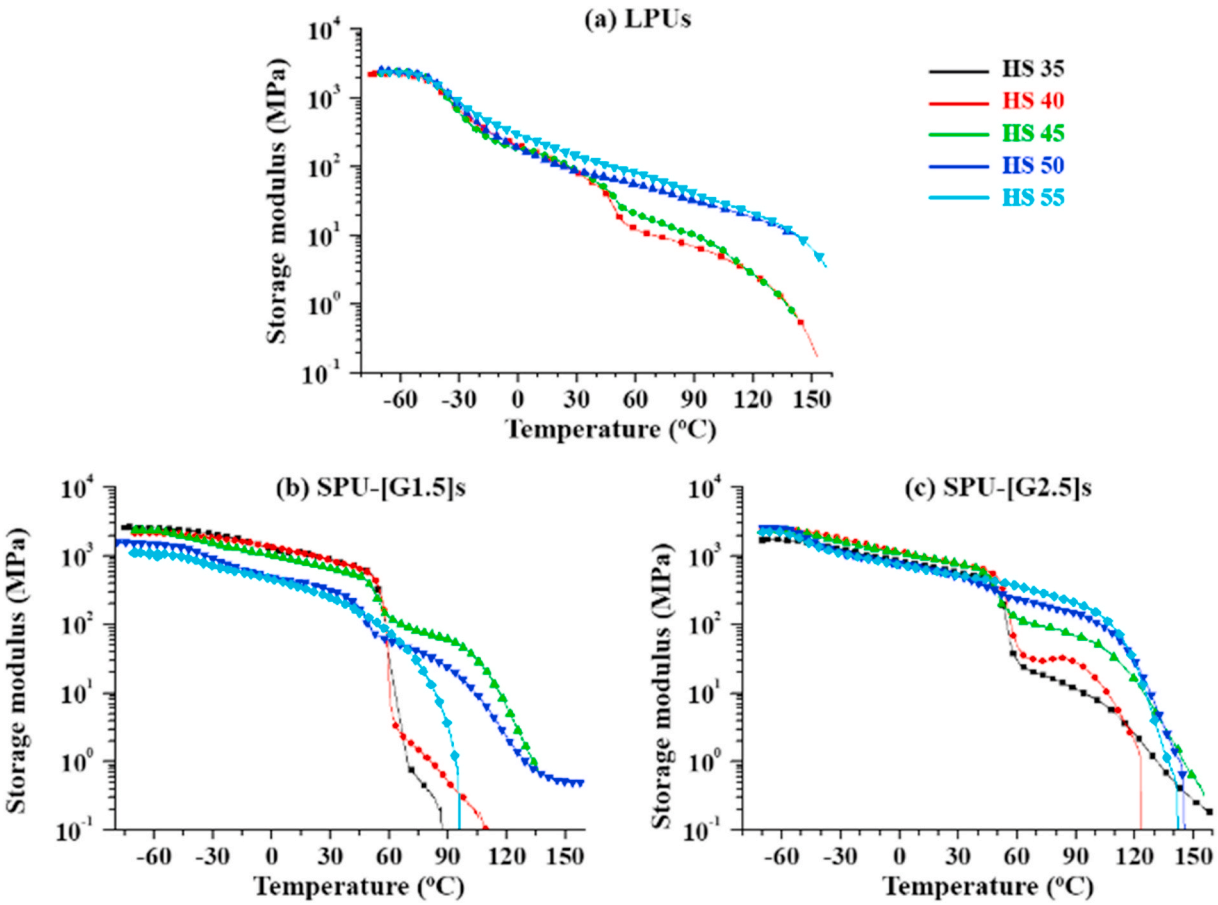

Fig. 4. Temperature dependence of the storage modulus at 1 Hz for (a) LPUs, (b) SPU-[G1.5]s and (c) SPU-[G2.5]s.

could freely organize into larger amorphous domains, while the above-mentioned domains were frozen by the crystallized HS (Fig. 3(e)). Moreover, the suppressed SS crystallization of second heating runs in DSC study implies the existence of amorphous HS as impurity in this amorphous SS-rich domain for LPUs. In Fig. 3(b)–(d), when the linear HS were replaced by branching units such as [G0.5]-ada, [G1.5]-ada, or [G2.5]-ada, the disappearance of melting transition indicates that the HS became amorphous at room temperature for SPU-[G0.5]s, SPU-[G1.5]s, and SPU-[G2.5]s. Due to the existence of amorphous HS, the growth of SS crystallinity grain sizes was observed as evidenced by the increased degree of crystallinity along with similar d-spacing between SPUs and typical TPUs (Fig. 3(b), (c), (d)). At 70 °C, various microphase separation morphologies were observed depending on the sizes of branching units. In Fig. 3(f), the nearly disappeared diffraction peak investigated by SAXS revealed a well mixing of HS and SS after the melting of SS for SPU-[G0.5]s. As the size of branching units increased (Fig. 3(g) and (h)), sharper peaks were observed and shifted to lower q territory in SAXS diffractions. This indicates that more distinct phase separation was created for SPU-[G1.5]s and SPU-[G2.5]s. With the further increased size of branching units, SPU-[G2.5]s exhibited purer microphase-separated domains in Fig. 3(h).

2.4. Mechanical properties

The temperature-dependent mechanical performance of the TPUs was studied by DMA (Fig. 4). In Fig. 4(a), the LPU samples exhibited a typical behavior of thermoplastic elastomeric polyurethanes. The sharp decrease in the storage modulus (E') around −35 °C with increasing temperature was attributed to the glass transition of the amorphous PCL-based SS. At about 60 °C, another sharp decrease in E' was due to the melting of SS crystals, especially for LPU40 and LPU45 with high SS crystallinity (Figure S15(a)). At temperature higher than 125 °C, the drop of E' was related to the melting of the HS domains.

When the pendant units were introduced into the TPU samples, SPU-[G0.5]s with weak intermolecular interactions were too fragile to be measured by DMA. The DMA results of SPU-[G1.5] and SPU-[G2.5] are shown in Fig. 4(b) and (c). In Fig. 4(b), SPU35-[G1.5], SPU40-[G1.5], and SPU45-[G1.5] with the higher SS crystallinity exhibited higher storage moduli than those of SPU50-[G1.5] and SPU55-[G1.5] below the SS melting temperature at about 60 °C. The drop of E' around −30 °C for SPU50-[G1.5] and SPU55-[G1.5] with lower SS crystallinity resulted from the glass transition of the amorphous SS. A sudden decrease in E' caused by the melting of SS was observed for the SPU-[G1.5]s around 60 °C, except the low-crystallinity SPU55-[G1.5] with a slow declining trend. In fact, SPU35-[G1.5] and SPU40-[G1.5] quickly softened at temperatures above 60 °C due to the low fraction of HS while E's of SPU45-[G1.5] and SPU50-[G1.5] reached a plateau above 60 °C, thanks to the physical crosslinking formed by the HS domains, and rapidly dropped at around 100 °C as the HS domains disintegrate [19,27,29]. Apart from that, SPU55-[G1.5] exhibited the lowest E' that dramatically decayed around 90 °C due to lack of both the SS crystallinity, and strong HS-SS incompatibility that would lead to distinct HS domains as cross-linking points. In Fig. 4(c), SPU35-[G2.5], SPU40-[G2.5], and SPU45-[G2.5] exhibited similar dynamic mechanical behaviors. Typically, the storage modulus, E' sharply decreased around 55 °C due to the melting of SS and then reached a plateau due to the HS physical cross-linking, followed by a liquification above 100 °C due to the disintegration of the HS domains. The storage modulus increased with increasing HS content. SPU50-[G2.5] and SPU55-[G2.5] with less SS crystallinity and high HS fractions exhibited a slight drop of E' around −50 °C, and

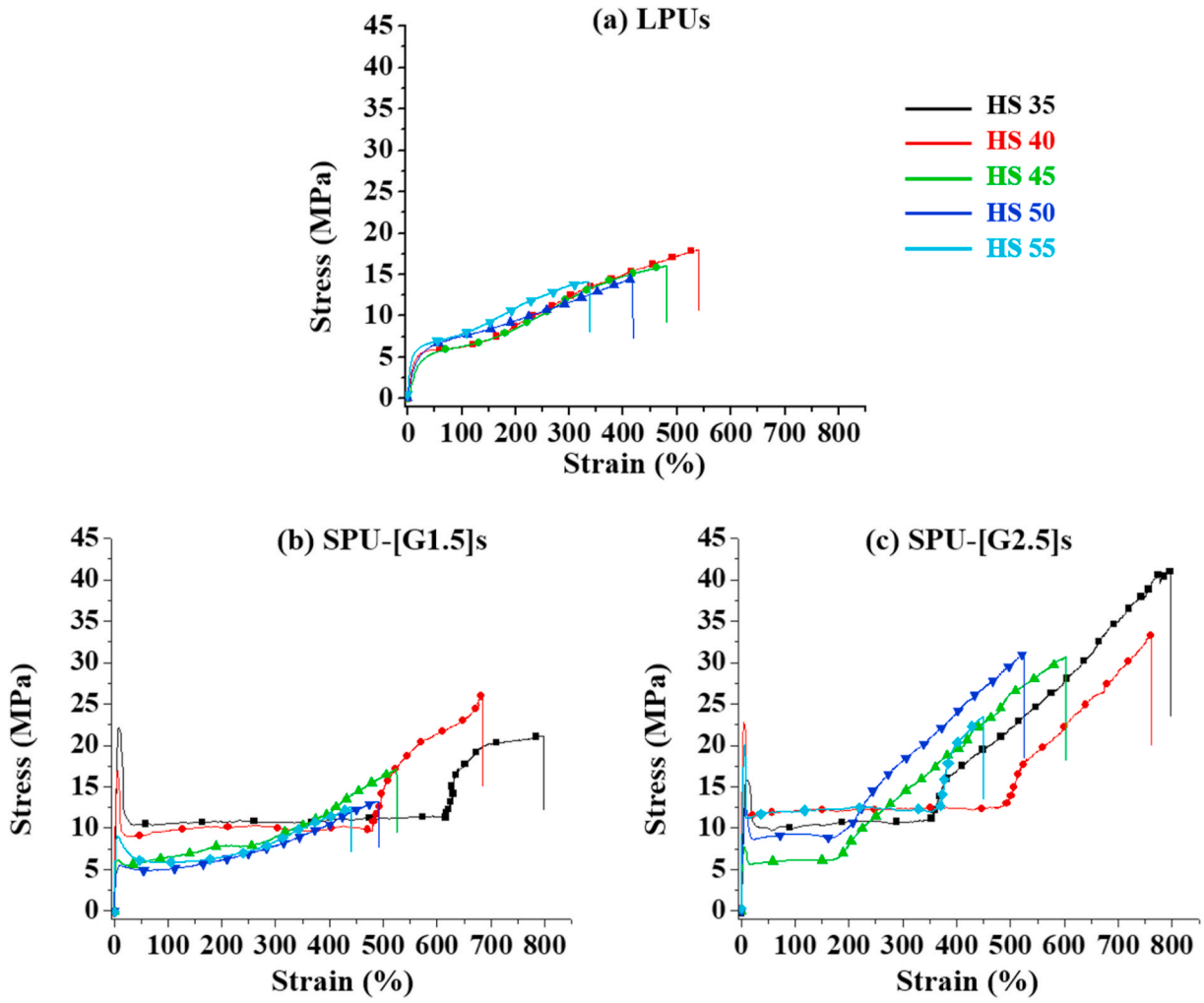

Fig. 5. Stress-strain curves for (a) LPUs, (b) SPU-[G1.5]s and (c) SPU-[G2.5]s.

then the storage modulus E' slowly decreased but remained higher than the rubbery plateau moduli of other SPU-[G2.5]s until a sharp drop above 100 °C. All SPU-[G2.5]s exhibited rubbery plateau regions between 50 and 100 °C, indicating that the dendron pendants of higher generations could effectively bring about the formation of stable HS domains that worked as the physical crosslinking points.

Fig. 5 shows the stress-strain curves for LPUs and SPUs. LPUs exhibited a typical elastomeric performance with over 300% elongation at break in the absence of the yield stress (Fig. 5(a)). The elongation at break increased with increasing SS content. As shown in Fig. 5(b) and (c), both SPU-[G1.5]s and SPU-[G2.5]s exhibited plastic-like behaviors with distinct yield stress and strain-hardening properties, which could be attributed to the existence of the high SS crystallinity. This yielding was mainly controlled by deformation within the crystals where a slip in crystal lamellae occurred. In addition, the stresses at breaks were improved with the growth of the pendant sizes because HS would form more robust physical crosslinking points. Among all the PUs, SPU35-[G2.5] exhibited the best performance, with a stress at break over 40 MPa and elongation at break over 750% (Fig. 5(c)).

2.5. Shape memory behavior

As mentioned in previous section, the EPU samples with low molecular weights and poor mechanical properties are not fit for shape memory test. Nevertheless, the LPUs and SPUs with robust mechanical properties were put to the tests. Shape memory performance was evaluated quantitatively by DMA in a force-controlled mode in the temperature range between 0 and 65 °C (Figure S20 and Table 2). The representative testing processes of TPUs with 40%HS are shown in Figure S21. In the first step, the specimens were equilibrated at 65 °C for

Table 2
Shape memory performance.

Sample[a]	Shape retention[b] (%)			Shape recovery[c] (%)		
	1st	2nd	3rd	1st	2nd	3rd
LPU35	83.1	82.3	84.6	77.5	66.8	62.3
LPU40	83.0	81.7	83.2	77.4	72.7	70.2
LPU45	82.3	82.0	82.2	76.9	70.4	70.3
LPU50	76.8	79.2	81.0	74.8	74.4	72.8
LPU55	75.9	73.2	76.0	73.6	73.5	72.8
SPU35-[G1.5]	98.6	98.7	98.9	94.2	88.1	78.8
SPU40-[G1.5]	98.8	98.7	98.7	94.8	89.9	84.5
SPU45-[G1.5]	97.8	97.8	97.8	95.2	90.9	86.0
SPU50-[G1.5]	90.1	90.6	89.2	91.8	86.6	83.0
SPU55-[G1.5]	90.9	92.1	89.5	90.9	84.9	81.9
SPU35-[G2.5]	98.7	99.0	98.3	96.8	94.2	94.1
SPU40-[G2.5]	98.0	98.4	98.6	98.4	97.5	97.2
SPU45-[G2.5]	97.9	97.7	97.8	96.2	95.9	95.4
SPU50-[G2.5]	93.6	94.4	91.2	95.7	93.3	92.3
SPU55-[G2.5]	88.2	82.6	82.0	91.1	86.2	85.1

[a] 100% deformation at 65 °C.
[b] Temporary shape retention at 0 °C.
[c] Shape recovery at 65 °C.

20 min without loading, which is above the melting temperature of SS but below the disintegration temperature of HS domains. Subsequently, the samples were stretched to a strain of 100% ($\varepsilon_m = 100\%$) under a force of 0.05 N/min. After the stretching, the specimens were cooled down to 0 °C at a rate of 5 °C/min. In the third step, the force was released, and the specimens were loaded with a minimal tensile force of 0.001 N and held isothermally at 0 °C for 10 min, which is considered as a stress-free condition where the equilibrium strain (ε_u) was recorded. In the final stage, the specimens were heated to 65 °C at 5 °C/min to complete one cycle of shape memory test and the strain (ε_p) after recovery was obtained [53–55]. The parameters of the shape memory performance are defined as follows:

$$\text{Shape retention ratio } (\%) = \varepsilon_u / \varepsilon_m \times 100.$$

$$\text{Shape recovery ratio } (\%) = (\varepsilon_m - \varepsilon_p) / \varepsilon_m \times 100.$$

For the LPU40 sample with elastomeric properties (Figure S21), the strain abruptly shrank after the force was released at 0 °C, indicating the SS crystallinity is not high enough to freeze the chain mobility and to maintain the strain. When the sample was heated up back to 65 °C, the recovery of strain stopped at 20–40% due to the weak HS physical crosslinks. The shape retention ratio ~70–85% and the shape recovery ratio ~60–80% shown in Table 2 indicate a poor shape memory performance for LPUs. The fixity of the strain after cooling and the recovery of the strain after reheating for SPU40-[G1.5] and SPU40-[G2.5] with high SS crystallinity and strong HS domains were greatly improved. The shape retention ratio and the shape recovery ratio of SPU40-[G2.5] were over 98% and stably maintained after three cycles of the shape memory test. SPU40-[G1.5] exhibited a relatively low shape recovery due to the somewhat weaker HS physical crosslinks. All in all, the shape memory performances of SPUs listed in Table 2 are much superior to those of LPUs, manifesting the significant role of the adamantyl dendrons in TPUs.

3. Conclusion

In this study, a unique approach to render the phase separation resulting in the unique structure-properties relationship for the versatile thermoplastic polyurethanes. Surprisingly, the reaction between 1-adamantanamine and azetidine-2,4-dione was restricted due to steric hindrance. Through our painstaking effort, this resulted in an isolated yield over 90% for a series of the adamantane containing poly (urea/malonamides) with well-defined structures. Unlike the typical thermal plastic polyurethanes with co-existence of crystallinity in both SS and HS domains, the introduction of the dendritic adamantane containing poly (urea/malonamides) provided an amorphous HS with high degree of SS crystallinity in the evidence of DSC and WXRD investigations. Depending on the sizes of branching architectures, which were determined by the use of different dendritic chain extenders of generation 0.5 to 2.5, distinguished microphase separation revealed that the highly branching HS would be able to create more physical crosslinking junctions at temperatures higher than the melting of SS as investigated by the temperature-dependent SAXs measurements. This phase separation characteristic created unique structure-properties relationship with sharp melting transitions and lengthy rubbery plateaus for the samples with larger branched HS components. As a result, thermoplastic polyurethanes of SPU40-[G2.5] exhibited a shape retention over 98%, and a shape recovery of 98% after three runs of the shape memory evaluations. This work demonstrates that the molecular engineering can significantly tailor the microstructures and properties on thermal plastic polymer.

CRediT authorship contribution statement

Chien-Hsin Wu: Conceptualization, Methodology, Software, Writing - original draft. **Ying-Chi Huang:** Data curation, Investigation. **Wei-Lun Chen:** Investigation, Data curation. **Yen-Yu Lin:** Investigation. **Shenghong A. Dai:** Supervision. **Shih-Huang Tung:** Writing - review & editing, Supervision. **Ru-Jong Jeng:** Writing - review & editing, Supervision.

Declaration of competing interest

The authors declare that they have no known competing financial have appeared to influence the work reported in this paper.

Acknowledgment

This work was financially supported by the ''Advanced Research Center of Green Materials Science and Technology'' from The Featured Area Research Center Program within the framework of the Higher Education Sprout Project by the Ministry of Education (109L9006) and the Ministry of Science and Technology in Taiwan (MOST 106-2218-E-002-021-MY3, MOST 108-3116-F- 002–008, MOST 109-2634-F-002 -042 and MOST 109-2622-8-006-005).

Appendix A. Supplementary data

Supplementary data to this article can be found online at https://doi.org/10.1016/j.polymer.2020.123075.

References

[1] C.R. McNeill, S. Westenhoff, C. Groves, R.H. Friend, N.C. Greenham, Influence of nanoscale phase separation on the charge generation dynamics and photovoltaic performance of conjugated polymer Blends: balancing charge generation and separation, J. Phys. Chem. C 111 (51) (2007) 19153–19160.
[2] K. Gao, S.B. Jo, X. Shi, L. Nian, M. Zhang, Y. Kan, F. Lin, B. Kan, B. Xu, Q. Rong, L. Shui, F. Liu, X. Peng, G. Zhou, Y. Cao, A.K.-Y. Jen, Over 12% efficiency nonfullerene all-small-molecule organic solar cells with sequentially evolved multilength scale morphologies, Adv. Mater. 31 (12) (2019), 1807842.
[3] M. Seo, M.A. Hillmyer, Reticulated nanoporous polymers by controlled polymerization-induced microphase separation, Science 336 (6087) (2012) 1422–1425.
[4] M.W. Schulze, L.D. McIntosh, M.A. Hillmyer, T.P. Lodge, High-modulus, high-conductivity nanostructured polymer electrolyte membranes via polymerization-induced phase separation, Nano Lett. 14 (1) (2014) 122–126.
[5] Z. Zhou, T. Liu, A.U. Khan, G. Liu, Block copolymer–based porous carbon fibers, Science Advances 5 (2) (2019), eaau6852.
[6] D.-J. Lee, T. Uryu, Synthesis of enantiotropic liquid crystal copolyurethanes containing para- and meta-type diisocyanate units in the backbone, Macromolecules 31 (21) (1998) 7142–7148.
[7] C. Gong, H.W. Gibson, Controlling polymeric topology by polymerization Conditions: mechanically linked network and branched poly(urethane rotaxane)s with controllable polydispersity, J. Am. Chem. Soc. 119 (37) (1997) 8585–8591.
[8] C.-H. Wu, Y.-R. Lin, S.-C. Yeh, Y.-C. Huang, K.-H. Sun, Y.-F. Shih, W.-C. Su, C.-A. Dai, S.A. Dai, R.-J. Jeng, A facile synthetic route to ether diols derived from 1,1-cyclopentylenylbisphenol for robust cardo-type polyurethanes, Macromolecules 52 (3) (2019) 959–967.
[9] S. Velankar, S.L. Cooper, Microphase separation and rheological properties of polyurethane melts. 1. Effect of block length, Macromolecules 31 (26) (1998) 9181–9192.
[10] R.M. Versteegen, R.P. Sijbesma, E.W. Meijer, [n]-Polyurethanes: synthesis and characterization, Angew. Chem. Int. Ed. 38 (19) (1999) 2917–2919.
[11] B.K. Kim, S.Y. Lee, M. Xu, Polyurethanes having shape memory effects, Polymer 37 (26) (1996) 5781–5793.
[12] P. Ping, W. Wang, X. Chen, X. Jing, Poly(ε-caprolactone) polyurethane and its shape-memory property†, Biomacromolecules 6 (2) (2005) 587–592.
[13] M.V. Pandya, D.D. Deshpande, D.G. Hundiwale, Effect of diisocyanate structure on viscoelastic, thermal, mechanical and electrical properties of cast polyurethanes, J. Appl. Polym. Sci. 32 (5) (1986) 4959–4969.
[14] L.L. Harrell, Segmented Polyurethans, Properties as a funcation of segment size and distribution, Macromolecules 2 (6) (1969) 607–612.
[15] C.D. Eisenbach, T. Heinemann, Thermoplastic graft copolymer elastomers with chain-folding or bifurcated side chains, Macromol. Chem. Phys. 196 (8) (1995) 2669–2686.
[16] C.D. Eisenbach, T. Heinemann, A. Ribbe, E. Stadler, Chain architecture and molecular self-organization of polyurethanes: perspectives for thermoplastic elastomers, Die Angewandte Makromolekulare Chemie 202 (1) (1992) 221–241.
[17] C.D. Eisenbach, T. Heinemann, Synthesis and characterization of thermoplastic graft copolymer elastomers with a polyether main chain and uniform urethane-based side chains, Macromolecules 28 (7) (1995) 2133–2139.
[18] S. Jahromi, V. Litvinov, B. Coussens, Polyurethane networks bearing dendritic Wedges: synthesis and some properties, Macromolecules 34 (4) (2001) 1013–1017.

[19] C.-H. Wu, Y.-C. Chen, S.A. Dai, S.-C. Chen, S.-H. Tung, R.-H. Lee, W.-C. Su, R.-J. Jeng, Iterative synthesis of monodisperse pendants for making comb-like polyurethanes, Polymer 119 (2017) 1–12.
[20] Y.-T. Chern, H.-C. Shiue, Low dielectric constants of soluble polyimides based on adamantane, Macromolecules 30 (16) (1997) 4646–4651.
[21] S.-H. Hsiao, C.-T. Li, Synthesis and characterization of new adamantane-based polyimides, Macromolecules 31 (21) (1998) 7213–7217.
[22] F. Zou, H. Chen, S. Fu, S. Chen, Shape memory materials based on adamantane-containing polyurethanes, RSC Adv. 8 (45) (2018) 25584–25591.
[23] S. Okamoto, S. Onoue, M. Kobayashi, A. Sudo, Rigid triol and diol with adamantane-like core derived from naturally occurring myo-inositol and their polyaddition with diisocyanates, J. Polym. Sci., Part A: Polym. Chem. 52 (24) (2014) 3498–3505.
[24] S. Fu, J. Zhu, S. Chen, Tunable shape memory polyurethane networks cross-linked by 1,3,5,7-tetrahydroxyadamantane, Macromol. Res. 26 (11) (2018) 1035–1041.
[25] Z.R. Lau, S.L. Sin, H. Yan, J.W. Xu, Adamantane-modified polyurethanes: effect of hydroxy group of adamantane on the properties of polyurethanes, Adv. Mater. Res. 1110 (2015) 92–95.
[26] S. Fu, J. Zhu, F. Zou, X. Zeng, S. Chen, A novel adamantane-based polyurethane with shape memory effect, Mater. Lett. 229 (2018) 44–47.
[27] C.-P. Chen, S.A. Dai, H.-L. Chang, W.-C. Su, T.-M. Wu, R.-J. Jeng, Polyurethane elastomers through multi-hydrogen-bonded association of dendritic structures, Polymer 46 (25) (2005) 11849–11857.
[28] C.-P. Chen, S.A. Dai, H.-L. Chang, W.-C. Su, R.-J. Jeng, Facile approach to polyurea/malonamide dendrons via a selective ring-opening addition reaction of azetidine-2,4-dione, J. Polym. Sci., Part A: Polym. Chem. 43 (3) (2005) 682–688.
[29] S.A. Dai, C.-P. Chen, C.-C. Lin, C.-C. Chang, T.-M. Wu, W.-C. Su, H.-L. Chang, R.-J. Jeng, Novel side-chain dendritic polyurethanes based on hydrogen bonding rich polyurea/malonamide dendrons, Macromol. Mater. Eng. 291 (4) (2006) 395–404.
[30] C.-H. Wu, S.-M. Shau, S.-C. Liu, S.A. Dai, S.-C. Chen, R.-H. Lee, C.-F. Hsieh, R.-J. Jeng, Enhanced shape memory performance of polyurethanes via the incorporation of organic or inorganic networks, RSC Adv. 5 (22) (2015) 16897–16910.
[31] C.-C. Tsai, C.-C. Chang, C.-S. Yu, S.A. Dai, T.-M. Wu, W.-C. Su, C.-N. Chen, F.M. C. Chen, R.-J. Jeng, Side chain dendritic polyurethanes with shape-memory effect, J. Mater. Chem. 19 (44) (2009) 8484–8494.
[32] S.A. Dai, T.-Y. Juang, C.-P. Chen, H.-Y. Chang, W.-J. Kuo, W.-C. Su, R.-J. Jeng, Synthesis of N-aryl azetidine-2,4-diones and polymalonamides prepared from selective ring-opening reactions, J. Appl. Polym. Sci. 103 (6) (2007) 3591–3599.
[33] C.-C. Tsai, T.-Y. Juang, S.A. Dai, T.-M. Wu, W.-C. Su, Y.-L. Liu, R.-J. Jeng, Synthesis and montmorillonite-intercalated behavior of dendritic surfactants, J. Mater. Chem. 16 (21) (2006) 2056–2063.
[34] M.-C. Kuo, S.-M. Shau, J.-M. Su, R.-J. Jeng, T.-Y. Juang, S.A. Dai, Preparation of supramolecular extenders with precise chain lengths via iterative synthesis and their applications in polyurethane elastomers, Macromolecules 45 (13) (2012) 5358–5370.
[35] C.-H. Wu, W.-H. Ting, Y.-W. Lai, S.A. Dai, W.-C. Su, S.-H. Tung, R.-J. Jeng, Tailored honeycomb-like polymeric films based on amphiphilic poly(urea/malonamide) dendrons, RSC Adv. 6 (94) (2016) 91981–91990.
[36] M.-C. Kuo, R.-J. Jeng, W.-C. Su, S.A. Dai, Iterative synthesis of extenders of uniform chain lengths for making thermo-reversible polyurethane supramolecules, Macromolecules 41 (3) (2008) 682–690.
[37] A. Lendlein, R. Langer, Biodegradable, elastic shape-memory polymers for potential biomedical applications, Science 296 (5573) (2002) 1673–1676.
[38] P. Ping, W. Wang, X. Chen, X. Jing, Poly(ε-caprolactone) polyurethane and its shape-memory property, Biomacromolecules 6 (2) (2005) 587–592.
[39] C.M. Yakacki, R. Shandas, D. Safranski, A.M. Ortega, K. Sassaman, K. Gall, Strong, tailored, biocompatible shape-memory polymer networks, Adv. Funct. Mater. 18 (16) (2008) 2428–2435.
[40] E. Delebecq, J.-P. Pascault, B. Boutevin, F. Ganachaud, On the versatility of urethane/urea bonds: reversibility, blocked isocyanate, and non-isocyanate polyurethane, Chem. Rev. 113 (1) (2013) 80–118.
[41] M. Hutchby, C.E. Houlden, J.G. Ford, S.N.G. Tyler, M.R. Gagné, G.C. Lloyd-Jones, K.I. Booker-Milburn, Hindered ureas as masked isocyanates: facile carbamoylation of nucleophiles under neutral conditions, Angew. Chem. Int. Ed. 48 (46) (2009) 8721–8724.
[42] Y. Zhao, Y. Chen, C. Chen, F. Xi, Synthesis of well-defined star polymers and star block copolymers from dendrimer initiators by atom transfer radical polymerization, Polymer 46 (15) (2005) 5808–5819.
[43] Y. Zhao, X. Shuai, C. Chen, F. Xi, Synthesis and characterization of star-shaped poly (l-lactide)s initiated with hydroxyl-terminated poly(amidoamine) (PAMAM-OH) dendrimers, Chem. Mater. 15 (14) (2003) 2836–2843.
[44] I.J. Majoros, B. Keszler, S. Woehler, T. Bull, J.R. Baker, Acetylation of poly (amidoamine) dendrimers, Macromolecules 36 (15) (2003) 5526–5529.
[45] X. Shi, I. Bányai, M.T. Islam, W. Lesniak, D.Z. Davis, J.R. Baker, L.P. Balogh, Generational, skeletal and substitutional diversities in generation one poly (amidoamine) dendrimers, Polymer 46 (9) (2005) 3022–3034.
[46] M.D. McKenna, J. Barberá, M. Marcos, J.L. Serrano, Discotic liquid crystalline poly (propylene imine) dendrimers based on triphenylene, J. Am. Chem. Soc. 127 (2) (2005) 619–625.
[47] J. Nithyanandhan, N. Jayaraman, Synthesis of Poly(alkyl aryl ether) Dendrimers, J. Org. Chem. 67 (17) (2002) 6282–6285.
[48] S.L. Cooper, A.V. Tobolsky, Properties of linear elastomeric polyurethanes, J. Appl. Polym. Sci. 10 (12) (1966) 1837–1844.
[49] C.S.P. Sung, N.S. Schneider, Temperature dependence of hydrogen bonding in toluene diisocyanate based polyurethanes, Macromolecules 10 (2) (1977) 452–458.
[50] A. Sarasam, S.V. Madihally, Characterization of chitosan–polycaprolactone blends for tissue engineering applications, Biomaterials 26 (27) (2005) 5500–5508.
[51] A. Saiani, W.A. Daunch, H. Verbeke, J.W. Leenslag, J.S. Higgins, Origin of multiple melting endotherms in a high hard block content polyurethane. 1. Thermodynamic investigation, Macromolecules 34 (26) (2001) 9059–9068.
[52] I. Navarro-Baena, J.M. Kenny, L. Peponi, Crystallization and thermal characterization of biodegradable tri-block copolymers and poly(ester-urethane)s based on PCL and PLLA, Polym. Degrad. Stabil. 108 (2014) 140–150.
[53] J. Hu, Z. Yang, L. Yeung, F. Ji, Y. Liu, Crosslinked polyurethanes with shape memory properties, Polym. Int. 54 (5) (2005) 854–859.
[54] K. Paderni, S. Pandini, S. Passera, F. Pilati, M. Toselli, M. Messori, Shape-memory polymer networks from sol–gel cross-linked alkoxysilane-terminated poly (ε-caprolactone), J. Mater. Sci. 47 (10) (2012) 4354–4362.
[55] L. Xue, S. Dai, Z. Li, Synthesis and characterization of three-arm poly (ε-caprolactone)-based poly(ester−urethanes) with shape-memory effect at body temperature, Macromolecules 42 (4) (2009) 964–972.